

# X-ray and lensing results on the cluster around the powerful radio galaxy 4C+55.16

K. Iwasawa<sup>1</sup>, S.W. Allen<sup>1</sup>, A.C. Fabian<sup>1</sup>, A.C. Edge<sup>2</sup> and S. Ettori<sup>1</sup>

<sup>1</sup> *Institute of Astronomy, Madingley Road, Cambridge CB3 0HA*

<sup>2</sup> *Department of Physics, University of Durham, South Road, Durham DH1 3LE*

## ABSTRACT

We present results from ASCA and ROSAT HRI observations of the powerful radio galaxy 4C+55.16 at redshift 0.24. Extended soft X-ray emission is imaged by the ROSAT HRI. The X-ray brightness profile is sharply peaked on the radio galaxy, characteristic of a strong cooling flow. The X-ray spectrum obtained from ASCA is consistent with multi-phase intracluster gas. There is evidence for an absorbed cool component as well as ambient cluster medium in the ASCA spectrum. A spectral fit, taking a cooling-flow component into account, gives a temperature of  $kT = 5.4^{+1.4}_{-0.9}$  keV, metal abundance  $(0.5 \pm 0.1)Z_{\odot}$ , excess absorption on the cool component,  $\Delta N_{\text{H}} = 4.9^{+3.4}_{-1.3} \times 10^{21} \text{cm}^{-2}$ , and an absorption-corrected bolometric luminosity of  $2.2 \times 10^{45} \text{erg s}^{-1}$  ( $H_0 = 50 \text{ km s}^{-1} \text{ Mpc}^{-1}$ ,  $q_0 = 0.5$ ). The mass deposition rate is estimated to be  $\sim 1100 M_{\odot} \text{ yr}^{-1}$  from the spectral analysis, in good agreement with that derived from imaging analysis of the ROSAT data when corrected for absorption. We tentatively identify a blue feature, seen  $\sim 15$  arcsec from the centre of the radio galaxy in a published optical image, as a gravitationally-lensed arc. The inferred lensing mass is consistent with the gravitational mass derived from the X-ray data. The best-estimate of the redshift of the lensed object is  $\sim 1.5 (> 0.7)$ . All the observed properties suggest that the environment of 4C+55.16 is similar to known massive cooling flow clusters. This is the first massive cooling flow to be found around a powerful, radio source with a compact, GHz-peaked spectrum core.

**Key words:** galaxies: clusters: individual: 4C+55.16 – X-rays: galaxies – cooling flows – gravitational lensing

## 1 INTRODUCTION

4C+55.16 (= 0831+557) is a radio galaxy at a redshift of 0.240 (Lawrence et al 1996) in the Pearson-Readhead (1981, 1988) 5 GHz flux-density-limited complete sample. The radio source is compact and powerful ( $1.1 \times 10^{26} \text{W Hz}^{-1} \text{sr}^{-1}$  at 5 GHz). In the high resolution radio maps obtained from MERLIN and VLBI (Whyborn et al 1985; Pearson & Readhead 1988), highly irregular, small-scale structures have been resolved. The radio spectrum of the compact core shows a turnover around 1 GHz (Component C in Whyborn et al 1985), resembling the class of Giga-hertz Peaked Spectrum (GPS) sources (e.g., O’Dea 1998) whilst the mini double-lobe with a projected size of  $11''$  (54 kpc at a redshift of 0.24) has a steep, low-frequency spectrum. A sum of the two components results in a flat radio spectrum over the GHz range.

A blue continuum contributes  $\sim 50$  per cent of the light at 3850Å (Heckman et al 1983) and its optical emission-line

spectrum shows a medium ionization state (e.g., Heckman et al 1983 based on the  $[\text{OII}]\lambda 5007/[\text{OII}]\lambda 3727$  ratio; Whyborn et al 1985;  $[\text{OIII}]\lambda 5007/\text{H}\beta \sim 4$ , Lawrence et al 1996).

X-ray emission was detected during the ROSAT All Sky Survey (RX J08349+5534, Brinkmann et al 1995; Laurent-Muehle et al 1996; Bade et al 1998). The ROSAT papers assumed that the X-ray emission originates in an active nucleus residing in 4C+55.16. However, as our imaging and spectral study using the ROSAT HRI and ASCA data show below, the observed X-rays appear to be dominated by cluster emission surrounding the radio galaxy.

The optical CCD images of 4C+55.16 were obtained by Hutchings, Johnson & Pyke (1988) using the Canada-France-Hawaii Telescope (CFHT) with *B* and *R* filters. There is a blue feature about 15 arcsec southwest from the centre of the galaxy, which we tentatively identify as a gravitationally lensed arc. We find a good agreement between the cluster masses estimated from X-ray and lensing techniques.

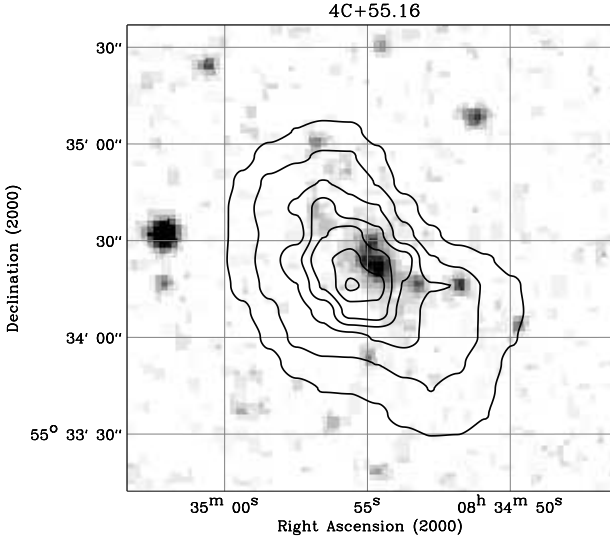


**Figure 1.** The X-ray (0.1–2.4 keV) contours of 4C+55.16 obtained from the ROSAT HRI image overlaid onto the optical DSS image taken by Palomar 48-inch Oschin Schmidt Telescope. The DSS image is not deep enough to show the arc-like feature detected in the CFHT image (Hutchings et al 1988). Contour levels are 6, 10, 16, 25, 40, 63, 95 per cent of the peak brightness which is 63 ct pixel<sup>-1</sup>. The estimated average background is about 1.3 ct pixel<sup>-1</sup>.

## 2 OBSERVATIONS AND DATA REDUCTION

4C+55.16 was observed with ASCA (Tanaka, Inoue & Holt 1994) and ROSAT HRI (Pfeffermann et al 1987). ASCA provides moderate resolution imaging and spectra in the 0.5–10 keV band while the ROSAT HRI provides high resolution (FWHM  $\sim 5$  arcsec) 0.1–2.4 keV imaging. A summary of the observations is given in Table 1.

The four detectors onboard ASCA, the Solid state Imaging Spectrometers (SIS; S0 and S1), the Gas Imaging Spectrometers (GIS; G2 and G3) were operating normally. The radio galaxy was pointed at the nominal position on the best-calibrated CCD chip of each SIS detector. The lowest energy event threshold in the SIS was set at 0.47 keV. Standard calibration (used for the Rev2 processing) and data reduction techniques were employed, using FTOOLS (version 4.0) provided by the ASCA Guest Observer Facility at Goddard Space Flight Center. The SIS data were corrected for the effects of the Dark Frame Error (DFE) and ‘Echo’ and hot/flickering pixels were removed.

The ROSAT HRI observation was short (16.6 ks). The soft X-ray image revealed extended X-ray emission which could not be resolved with ASCA (Section 3). The data were also analysed by the deprojection technique (Section 5). There is no evidence for X-ray variation in both ASCA and ROSAT data.

## 3 THE ROSAT HRI IMAGE

The X-ray source detected at the position of 4C+55.16 is clearly extended beyond the Point Spread Function (PSF)

of the HRI. The raw HRI image has been smoothed with the adaptive kernel method, ASMOOTH (Ebeling, White & Rangarajan 1998), using a gaussian kernel and a characteristic smoothing threshold, above the local background, of  $4\sigma$ . Fig. 1 shows the X-ray intensity contours of the smoothed data overlaid on the optical Digitized Sky Survey (DSS) image.

The X-ray emission is sharply peaked at the centre of the extended image, as observed in strong cooling flow clusters. The X-ray peak is displaced from the galaxy nucleus by  $\sim 7$  arcsec, well within the mean displacement (25 arcsec) between X-ray and optical peaks seen in cooling flow clusters observed with ROSAT HRI (Peres et al 1997). Although the displacement is consistent with the positional uncertainty of ROSAT pointing ( $\sim 10$  arcsec), if it is real the galaxy resides in the X-ray cavity, as seen in the Perseus cluster (Böhringer et al 1993). There are three point-like sources detected in the HRI field. One of them shows an offset from a possible optical counterpart, similar in amplitude and direction to that for 4C+55.16. Therefore the displacement between X-ray and optical peaks may be merely due to a pointing error.

The elongation of the X-ray image is prominent at the low surface brightness levels. However, this may be partly due to a contamination from point sources in the field, particularly in the SW region. The present observation is too short to investigate such a faint X-ray morphology.

## 4 THE ASCA X-RAY SPECTRUM

The spectral analysis was performed using XSPEC (version 10.0). The MEKAL model (the original MEKA code, described by Kaastra 1992, with modified Fe-L line emissivity by Liedahl et al 1995) for an optically thin, collisional ionization equilibrium plasma was used with solar abundances taken from Anders & Grevesse (1989). The photoelectric absorption model was taken from Morrison & McCammon (1983). The Galactic absorption at the position of 4C+55.16 is estimated to be  $N_H = 4.2 \times 10^{20} \text{ cm}^{-2}$  from the HI measurements of Dickey & Lockman (1990). Absorption column densities obtained from the spectral fits are then excesses above the Galactic value. Quoted errors to the best-fit spectral parameters are 90 per cent confidence regions for one parameter of interest.

The ASCA spectrum shows a clear line feature at 5.4 keV, which is in an excellent agreement with the rest Fe K $\alpha$  line emission at  $\sim 6.7$  keV expected from a thin thermal plasma with a temperature of several keV at the redshift ( $z = 0.240$ ) of 4C+55.16. The agreement between the redshifts of the Fe K $\alpha$  line and the radio galaxy strongly supports the presence of a cluster around the radio galaxy rather than in the background which was suspected by Hutchings et al (1988). The thermal emission model (MEKAL) provides a slightly better fit to the data (0.6–9 keV from the SIS; 0.9–10 keV from the GIS) than the model of a power-law plus a gaussian line for the Fe K $\alpha$  line feature (see Table 2). The strong, narrow Fe K $\alpha$  line at 6.7 keV is unlikely for an active galaxy but naturally explained by thermal emission from cluster gas whose X-ray emission has been spatially resolved by the ROSAT HRI.

There is evidence for multi-phase gas in the ASCA

**Table 1.** The ASCA and ROSAT observations of 4C+55.16. No corrections for vignetting has been made for the count rates given here.

Satellite	Detector	Operation mode	Band	Date	Exposure ks	Count rate ct s <sup>-1</sup>
ASCA	SIS (S0/S1)	1CCD/Faint	0.5–10 keV	1996 Nov 1–2	34.5/34.0	0.12/0.10
	GIS (G2/G3)	PH	0.7–10 keV		38.1/37.8	0.065/0.078
ROSAT	HRI		0.1–2.4 keV	1997 Oct 20	16.5	0.062

**Table 2.** Spectral fits to the ASCA SIS (0.6–9 keV) and GIS (0.9–10 keV) data.  $\Delta N_{\text{H}}$  is the excess column density above the Galactic value ( $4.2 \times 10^{20} \text{ cm}^{-2}$ ), measured in the galaxy rest frame. Errors are quoted at the 90 per cent confidence level for one parameter of interest. In the model (a), the gaussian line energy is corrected for the galaxy redshift. The equivalent width of the line is  $520_{-138}^{+144}$  eV. In the thermal emission model (MEKAL), the Solar abundance table from Anders & Grevesse (1989) is used. In the model (c), the cool component is the cooling flow model with an initial temperature  $kT_i$ , metal abundane  $Z$  and a mass deposition rate of  $\dot{M}$ . The column density of cold absorption for the cool component ( $\Delta N_{\text{H,cool}}$ ) is measured at  $z = 0.24$ .

(a) Power-law plus a Gaussian line

$\Gamma$	$\Delta N_{\text{H}}$ $10^{21} \text{ cm}^{-2}$	$E$ keV	$\sigma$ keV	$I$ $10^{-5} \text{ ph s}^{-1} \text{ cm}^{-2}$	$\chi^2/\text{dof}$
$2.23_{-0.05}^{+0.07}$	$3.24_{-0.44}^{+0.54}$	$6.70_{-0.06}^{+0.05}$	$0(< 0.12)$	$1.65_{-0.43}^{+0.45}$	529.6/511

(b) Single thermal emission model (MEKAL)

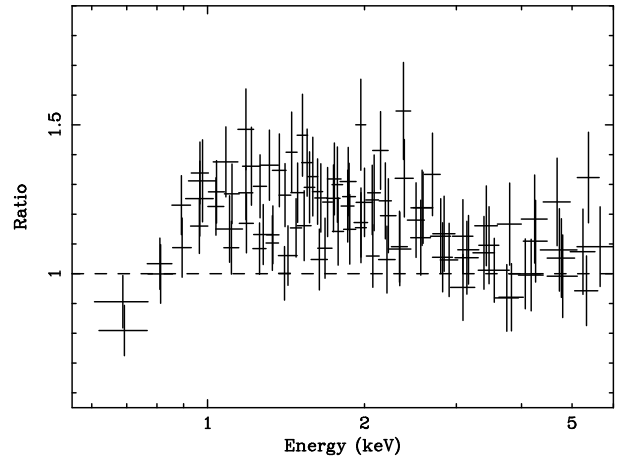
$kT$ keV	$Z$ $Z_{\odot}$	$\Delta N_{\text{H}}$ $10^{21} \text{ cm}^{-2}$	$\chi^2/\text{dof}$
$4.06_{-0.26}^{+0.27}$	$0.48_{-0.10}^{+0.11}$	$1.28_{-0.36}^{+0.38}$	521.8/513

(c) Multi-phase thermal emission model

$kT_i$ keV	$Z$ $Z_{\odot}$	$\dot{M}$ $M_{\odot} \text{ yr}^{-1}$	$\Delta N_{\text{H,cool}}$ $10^{21} \text{ cm}^{-2}$	$\chi^2/\text{dof}$
$5.4_{-0.9}^{+1.4}$	$0.49_{-0.12}^{+0.13}$	$1100_{-410}^{+240}$	$4.9_{-1.3}^{+3.4}$	524.0/512

spectrum. Fits to the ASCA data above and below 3 keV with a single thermal emission model (MEKAL) give significantly different values of temperature (Table 3). The data below 3 keV also require excess absorption ( $\Delta N_{\text{H}} = 0.98_{-0.32}^{+0.34} \times 10^{21} \text{ cm}^{-2}$  measured in the Earth frame) above the Galactic value. The extrapolation of the best-fit model for the 3–10 keV data leaves excess emission down to 1 keV followed by a decline towards 0.6 keV is probably due to absorption (Fig. 2). This indicates a multi-phase gas consisting of at least an absorbed, cool component with a less absorbed, ambient medium. This is characteristic of a cooling flow.

A fit to the whole band data (0.6–8 keV for the SIS; 0.9–10 keV for the GIS) with a multi-phase model (Model-c in Table 2), consisting of a single temperature MEKAL with Galactic absorption and the cooling flow model (Johnstone et al 1992) modified by extra absorption at the source, gives temperature, metal abundance, mass deposition rate and excess absorption column for the cooled component of  $kT = 5.4_{-0.9}^{+1.4}$  keV,  $Z = 0.50_{-0.13}^{+0.12} Z_{\odot}$ ,  $\dot{M} = 1100_{-410}^{+240} M_{\odot} \text{ yr}^{-1}$ , and  $N_{\text{H}} = 4.9_{-1.3}^{+3.4} \times 10^{21} \text{ cm}^{-2}$ , respectively. The temperature is listed for the ambient medium (i.e., before cooling), the metallicity is assumed to be identical between the two components, and the absorption column density is corrected for the galaxy redshift. The quality of the fit is acceptable and comparable to the single phase model (see Table 2). The

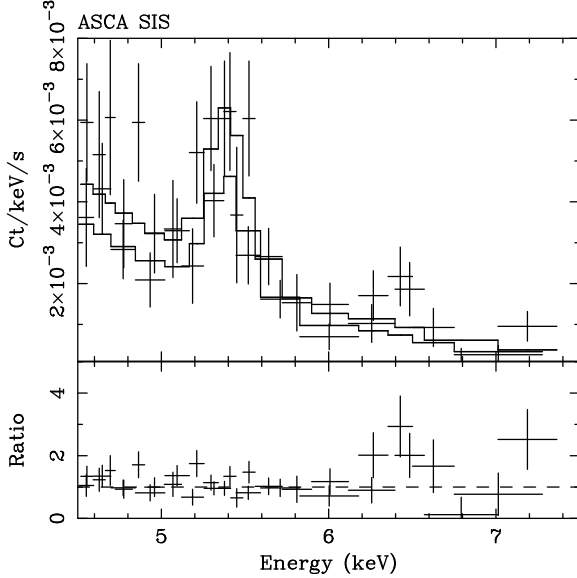
**Figure 2.** The ratio plot of the data and the extrapolation of the MEKAL model best-fitting the 3–10 keV data. Excess soft X-ray emission can be seen down to 1 keV and then it declines towards lower energies.

covering fraction of the cold absorption must be larger than 0.9 (90 per cent lower limit).

The observed fluxes in the 0.5–2 keV and 2–10 keV bands obtained from the GIS are  $1.72 \times 10^{-12} \text{ erg cm}^{-2} \text{ s}^{-1}$  and  $2.56 \times 10^{-12} \text{ erg cm}^{-2} \text{ s}^{-1}$ , respectively. In the best-fit

**Table 3.** Thermal emission model fits to the data above and below 3 keV.

Data	$kT$ keV	$Z$ $Z_{\odot}$	$\Delta N_{\text{H}}$ $10^{21} \text{cm}^{-2}$	$\chi^2/\text{dof}$
$E > 3 \text{ keV}$	$5.40^{+1.01}_{-0.81}$	$0.48^{+0.12}_{-0.11}$	0	151.4/156
$E < 3 \text{ keV}$	$3.73^{+0.71}_{-0.46}$	$0.59^{+0.37}_{-0.25}$	$0.98^{+0.34}_{-0.32}$	406.7/394

**Figure 3.** The Fe K band spectrum obtained from the ASCA SIS. The solid-line histogram represents the best-fit thermal emission model (See Table 3). Fe K $\beta$  emission around 6.4 keV (7.9 keV in the galaxy rest-frame) is detected with marginal significance above the model.

multi-phase model, about half of the total flux comes from the cool component.

Excess line-like emission at a rest energy of 7.9 keV (6.4 keV in the observed frame) is marginally detected in the SIS data (Fig. 3). It can be identified with Fe K $\beta$ . This feature is barely seen in the G3 data but not in the G2 data which show an unusual deficit between 6–7 keV, probably due to some anomaly in the detector. Since there is an instrumental feature at 6.4 keV in the SIS spectrum, the SIS results should be treated with caution. If the feature in the SIS data is real, the Fe K $\beta$  emission is underestimated by a factor of  $2.3 \pm 1.5$  by the best-fit thermal emission model. An anomalous Fe K $\beta$ /Fe K $\alpha$  ratio has been observed in the central region of a few cooling flow clusters, and has been interpreted as the effect of resonant scattering of line photons in the cluster core (e.g., Akimoto et al 1996; Molendi et al 1998). This interpretation is however not applicable to 4C+55.16 because the whole cluster emission is observed. Further deeper observations are required to confirm the existence of this emission feature.

## 5 DEPROJECTION ANALYSIS OF THE HRI DATA AND THE X-RAY MASS MODEL

We have carried out a deprojection analysis of the ROSAT HRI data. An azimuthally-averaged X-ray surface brightness

profile was constructed for the cluster. This was background-subtracted, corrected for telescope vignetting and re-binned into 12 arcsec bins to provide sufficient counts in each annulus for a reliable statistical analysis to be carried out. With the X-ray surface brightness profile as the primary input, and under assumptions of spherical symmetry and hydrostatic equilibrium, the deprojection technique yields the basic properties of the intracluster gas (temperature, density, pressure, cooling rate) as a function of radius.

The deprojection method requires the total mass profile for the cluster to be specified. We have iteratively determined the mass profile (which has been parameterized as an isothermal sphere; Equation 4-125 of Binney & Tremaine 1987) that results in a deprojected temperature profile which is isothermal within the region probed by the ROSAT data and which is consistent with the best-fit temperatures determined from the ASCA spectra, using the cooling-flow model (Section 4, The validity of the assumption of isothermal mass-weighted temperature profiles in the cluster cores is discussed by Allen 1998b). The best-fitting mass model has a core radius of  $60 \pm 20 \text{ kpc}$  and a velocity dispersion of  $820^{+100}_{-70} \text{ km s}^{-1}$ .

The primary results from the deprojection analysis are as follows: for an assumed Galactic column density of  $4.2 \times 10^{20} \text{ cm}^{-2}$ , we determine the mean cooling time within the central 12 arcsec bin of  $t_{\text{cool}} = 2.0^{+0.3}_{-0.2} \times 10^9 \text{ yr}$ , a cooling radius (beyond which the cooling time exceeds a Hubble time) of  $r_{\text{cool}} = 180^{+130}_{-40} \text{ kpc}$ , and an integrated mass deposition rate within the cooling radius of  $\dot{M} = 460^{+260}_{-140} M_{\odot} \text{ yr}^{-1}$ . If we correct for intrinsic absorption in the cluster, as determined from the ASCA data, these values are adjusted to  $t_{\text{cool}} = 1.5^{+0.2}_{-0.2} \times 10^9 \text{ yr}$ ,  $r_{\text{cool}} = 270^{+50}_{-10} \text{ kpc}$ , and  $\dot{M} = 970^{+270}_{-450} M_{\odot} \text{ yr}^{-1}$ .

## 6 LENSING ANALYSIS AND COMPARISON WITH THE X-RAY RESULTS

The mass model determined from the X-ray data may be compared to the mass implied by the observed lensing configuration in the cluster (Section 1). Since only a single, putative gravitational arc is seen, and to be consistent with the X-ray analysis, we have only carried out a simple, spherically-symmetric analysis of the lensing data. For a spherical mass distribution, the projected mass within the tangential critical radius, which we assume to be equal to the arc radius,  $r_{\text{arc}} = 15 \text{ arcsec}$  (71.8 kpc), is given by

$$M_{\text{arc}}(r_{\text{arc}}) = \frac{c^2}{4G} \left( \frac{D_{\text{arc}}}{D_{\text{clus}} D_{\text{arc-clus}}} \right) r_{\text{arc}}^2 \quad (1)$$

where  $D_{\text{clus}}$ ,  $D_{\text{arc}}$  and  $D_{\text{arc-clus}}$  are respectively the angular diameter distances from the observer to the cluster, the observer to the lensed object, and the cluster to the lensed

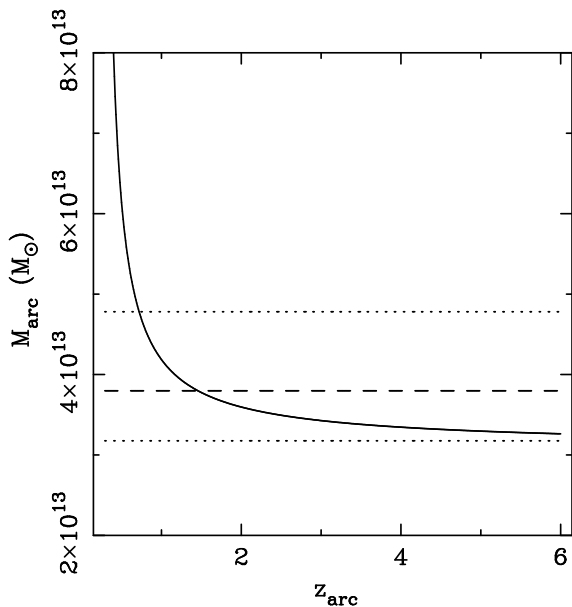


**Figure 4.** The projected lensing mass within the critical radius as a function of the redshift of the lensed object (solid curve). The gravitational mass estimated from the deprojection analysis using the ASCA results is indicated by a dashed line with the 90 per cent confidence limits shown by dotted lines.

object. Fig. 4 shows the projected mass within the critical radius as a function of the redshift of the arc (solid curve). The horizontal dashed and dotted lines mark the best fit (projected) mass measurement and 90 per cent confidence limits determined from the X-ray data, within the same radius ( $3.8^{+1.0}_{-0.6} \times 10^{13} M_{\odot}$ ). We see that the X-ray and lensing mass measurements are consistent for any arc redshift  $z_{\text{arc}} > 0.7$ . The best match between the X-ray and lensing mass measurements is obtained for an arc redshift of 1.5.

## 7 DISCUSSION

The ROSAT HRI image of the powerful radio galaxy 4C+55.16 shows extended X-ray emission peaking at the radio galaxy indicating cluster emission with a strong cooling flow.

A spectral study of the ASCA data suggests the X-ray emitting gas to be multi-phase. An absorbed, cool component is found in the spectrum. The multi-phase spectral analysis indicates that the temperature of the ambient cluster medium is  $kT \simeq 5.4$  keV. A single-phase model fitted to the data gives a temperature lower by  $\sim 1$  keV, typical of a cooling flow cluster.

The mass deposition rate of the cooling flow,  $1100^{+240}_{-410} M_{\odot} \text{ yr}^{-1}$ , derived from the spectral analysis is consistent with that ( $970^{+270}_{-450} M_{\odot} \text{ yr}^{-1}$ ) estimated from the image analysis when corrected for excess absorption. Agreements between mass deposition rates derived from the two methods have been found for other distant cooling-flow clusters (Allen 1998b).

The optical spectrum of 4C+55.16 (Lawrence et al 1996) is indeed very similar to the other cooling flow galax-

ies (Crawford et al 1999). The H $\alpha$  luminosity is about  $8 \times 10^{42} \text{ erg s}^{-1}$  (Lawrence et al 1996). The relatively large Balmer decrement (H $\alpha$ /H $\beta \simeq 5.5$ ) suggests a significant reddening, which is often observed in cooling flows. The inferred absorption column density is slightly smaller than observed in the X-ray spectrum.

The absorption-corrected 2–10 keV and bolometric luminosities, computed from the multi-phase model, are  $8.0 \times 10^{44} \text{ erg s}^{-1}$ , and  $2.2 \times 10^{45} \text{ erg s}^{-1}$ , respectively ( $H_0 = 50 \text{ km s}^{-1} \text{ Mpc}^{-1}$  and  $q_0 = 0.5$ ). About 60 per cent of the bolometric luminosity is due to the cooling flow. The bolometric luminosity exceeds that predicted for the single-phase temperature of 4 keV from the correlation between emission-weighted cluster temperature and luminosity (Mushotzky 1984; Edge & Stewart 1991; David et al 1993; Fabian et al 1994; Mushotzky & Sharf 1997; White et al 1997). A similar discrepancy is found for the other strong cooling flow clusters (e.g., Fabian et al 1994; Allen & Fabian 1998a; Markevich 1998). Taking the temperature derived from the multi-phase spectral analysis, 4C+55.16 fits well the  $kT_X$ – $L_{\text{Bol}}$  correlation obtained from a similar analysis of other luminous ( $L_{\text{Bol}} > 10^{45} \text{ erg s}^{-1}$ ) clusters for which the effect of cooling flows is included (Allen & Fabian 1998a), and is consistent with  $L_{\text{Bol}} \propto T_X^2$  expected from simple gravitational collapses for formation of clusters (Kaiser 1986; Navarro, Frenk & White 1995).

As shown in Section 6 (and Fig. 4), the mass estimated using the tentatively-identified lensing arc and the gravitational mass derived from the X-ray deprojection analysis are in good agreement. Moreover, the core radius of  $60 \pm 20$  kpc measured for 4C+55.16 is similar to the best-fit mean value of  $\sim 50$  kpc measured in the six lensing cooling-flow clusters studied by Allen (1998b).

The inferred metallicity of this cluster gas is  $\sim 0.5 Z_{\odot}$ , which is not unusual, but is certainly one of the higher values measured among the ASCA cluster sample compiled by Allen & Fabian (1998b). They showed that cooling-flow clusters show higher metallicity than non cooling-flow clusters, and suggest that the sharply peaked X-ray brightness profiles may give apparently high values of the emissivity-weighted metallicity in cooling flow clusters when there is a metallicity gradient in the cluster core. Thus the high metallicity in 4C+55.16 may be due to a steep metallicity gradient towards the cluster centre. The high metallicity measured in the spectrum also rules out significant contribution from the active nucleus to the observed hard X-ray emission around the Fe K band, otherwise the line would be less prominent.

We conclude that all of the available evidence points to the environment of 4C+55.16 being like other distant massive cooling flow clusters. 4C+55.16 is yet another powerful radio galaxy surrounded by a strong cooling flow. Unlike Cygnus A and 3C295, 4C+55.16 is a compact radio source. Detailed high spatial resolution observations with AXAF will be required to determine the interaction between the radio source and the dense surrounding intracluster medium. Probably the most comparable cluster to 4C+55.16 is PKS 0745–19, which also contains a strong cooling flow and exhibits gravitationally-lensed arcs (Allen, Fabian & Kneib 1996). However, the amorphous radio source shows a steep spectrum and is almost 2 orders of magnitude less powerful than 4C+55.16 at 5 GHz. Massive cooling flows

have not been found so far around ‘pure’ compact, GPS cores (e.g., O’Dea et al 1996).

The gas pressure at the centre of a cooling flow is  $P = nT \approx 10^7 \text{ cm}^{-3} \text{ K}$  (Heckman et al 1989). This leads to a free-free absorption optical depth  $\tau_{\text{ff}} \approx 0.6 P_7^2 \nu_9^{-2} T_4^{7/2} l_1$  at a frequency  $10^9 \nu_9 \text{ Hz}$ , through a cloud of length  $10 l_1 \text{ pc}$  at pressure  $10^7 P_7 \text{ cm}^{-3} \text{ K}$  and temperature  $10^4 T_4 \text{ K}$ . It is therefore plausible that the turnover seen in the radio spectrum of the compact core at  $\sim 1.7 \text{ GHz}$  (Whyborn et al 1985) is due to free-free absorption in the  $\text{H}\alpha$  emitting gas close to the nucleus. The covering fraction in such clouds must however decrease rapidly away from the nucleus in order that the radio knot observed  $\sim 100 \text{ pc}$  north-west of the nucleus (Whyborn et al 1985; Pearson & Readhead 1988) is not absorbed. The inverted spectrum of the counter-jet of NGC1275, which also resides in a cooling flow, is suspected to be due to free-free absorption on the pc scale (Vermeulen, Readhead, & Backer 1994). Free-free absorption is favoured for the spectral turnover in GPS sources by Begelman (1997) and Bicknell, Dopita & O’Dea (1997). Part of the observed optical emission-line luminosity from the innermost part of 4C+55.16 can be expected from shocked gas surrounding the jets of such a powerful and a relatively young radio source (e.g., Bicknell et al 1997), as well as from the cooling flow.

## ACKNOWLEDGEMENTS

We thank the ASCA and ROSAT teams for their efforts on operation of the satellites, and the calibration and maintenance of the software. The optical image we used in Fig. 1 was taken from the Digitized Sky Survey which was produced at the Space Telescope Science Institute (ST ScI) under U.S. Government grant NAG W-2166. We thank Royal Society (ACE, ACF, SE) and PPARC (KI, SWA) for support.

## REFERENCES

- Akimoto F., Tawara Y., Furuzawa A., Kumada A., Yamashita K., 1997, eds, F. Makino and K. Mitsuda, X-Ray Imaging and Spectroscopy of Cosmic Hot Plasmas, UAP Inc., Tokyo, p95
- Allen S.W., Fabian A.C., Kneib J.P., 1996, MNRAS, 279, 615
- Allen S.W., 1998a, MNRAS, submitted
- Allen S.W., 1998b, MNRAS, 296, 392
- Allen S.W., Fabian A.C., 1998a, MNRAS, 297, L57
- Allen S.W., Fabian A.C., 1998b, MNRAS, 297, L63
- Anders E., Grevesse N., 1989, Geochim. Cosmochim. Acta, 53, 197
- Bade H., et al, 1998, A&AS, 127, 145
- Begelman M.C., 1997, The Most Distant Galaxies, the KNAW Colloquium, Dordrecht: Reidel (astro-ph/9712107)
- Bicknell G.V., Dopita M.A., O’Dea C.P.O., 1997, ApJ, 485, 112
- Böhringer H., Voges W., Fabian A.C., Edge A.C., Neumann D.M., 1993, MNRAS, 264, L25
- Binney J., Tremaine S., 1987, Galactic dynamics, Princeton University Press, Princeton
- Brinkmann W., Siebert J., Reich W., Furst E., Reich P., Voges W., Trümper J., Wielebinski R., A&AS, 109, 147,
- David L.P., Slyz A., Jones C., Forman W., Vrtilik S.D., Arnaud K.A., 1993, 412, 479
- Dickey J.M., Lockman F.J., 1990, ARAA, 28, 215
- Edge A.C. Stewart G.C., 1991, MNRAS, 252, 414
- Fabian A.C., Crawford C.S., Edge A.C., Mushotzky R.F., 1994, MNRAS, 267, 779
- Heckman T.M., Lebofsky M.J., Rieke G.H., van Breugel W., 1983, ApJ, 272, 400
- Heckman T.M., Baum S.A., van Breugel W.J.M., McCarthy P., 1989, ApJ, 338, 48
- Hutchings J.B., Johnson I., Pyke R., 1988, ApJS, 66, 361
- Johnstone R.J., Fabian A.C., Edge A.C., Thomas P.A., 1992, MNRAS, 255, 431
- Kaastra J., 1992, An X-Ray Spectral Code for Optically Thin Plasmas (Internal SRON-Leiden Report, updated version 2.0)
- Kaiser N., 1986, MNRAS, 222, 323
- Liedahl D.A., Osterheld A.L., Godstein W.H., 1995, ApJ, 438, L115
- Lawrence C.R., Zucker J.R., Readhead A.C.S., Unwin S.C., Pearson T.J., Xu W., 1996, ApJS, 107, 541
- Laurent-Muehleisen S.A., Kollgaard R.I., Ryan P.J., Feigelson E.D., Brinkmann W., Siebert J., 1997, A&AS, 122, 235
- Molendi S., Matt G., Antonelli L.A., Fiore F., Fusco-Femiano R., Kaastra J., Maccarone C., Perola C., 1998, ApJ, 499, 608
- Markevich M., 1998, ApJ, 504, 27
- Morrison R., McCammon D.M., 1983, ApJ, 270, 119
- Mushotzky R.F., 1984, Phys. Scr., T7, 157
- Mushotzky R.F., Sharf C.A., 1997, ApJ, 482, L13
- Navarro J.F., Frenk C.S., White S.D.M., 1995, MNRAS, 275, 720
- O’Dea C.P., 1998, PASP, 110, 493
- Pearson T.J., Readhead A.C.S., 1988, ApJ, 328, 114
- Pearson T.J., Readhead A.C.S., 1981, ApJ, 248, 61
- Peres C.B., Fabian A.C., Edge A.C., Allen S.W., Johnstone R.M., White D.A., 1998, MNRAS, 298, 416
- Tanaka Y., Inoue H., Holt S.S., 1994, PASJ, 46, L37
- Vermeulen R.C., Readhead A.C.S., Backer D.C., 1994, ApJ, 430, L41
- White D.A., Jones C., Forman W., 1997, MNRAS, 292, 419
- Whyborn N.D., Browne I.W.A., Wilkinson P.N., Porcas R.W., Spinrad H., 1985, MNRAS, 214, 55